

SCBSS Signal De-Noising Method of Integrating EEMD and ESMD for Dynamic Deflection of Bridges Using GBSAR

Xianglei Liu¹, Hui Wang, and Yimeng Huang

Abstract—Ground-based synthetic aperture radar (GBSAR) technology, as a new measurement technology, has the advantages of noncontact measurements, high precision, and all-weather measurement capability, and it has been widely used for bridge dynamic deflection measurements. In order to reduce the influence of noise in dynamic deflection of bridges obtained using GBSAR, this article proposes a single-channel blind source separation signal (SCBSS) de-noising method to obtain the denoised dynamic deflection of bridges. First, the extreme-point symmetric mode decomposition (ESMD) method and the ensemble empirical mode decomposition (EEMD) method are used to decompose the obtained dynamic deflection—as the original observation signal—into a series of intrinsic mode functions (IMFs) and a residual R . Second, the Spearman's Rho of each IMF with the original observation signal is calculated to remove the dominant IMFs of high-frequency noise. Third, the remaining IMFs and R decomposed by ESMD and EEMD are reconstructed into two sets of new signals, which form a new virtual multichannel data with the original observation signal. Finally, blind source separation is performed on the new virtual multichannel signal to obtain separated signal components. The separate signal components are converted in the frequency domain using the fast Fourier transform algorithm, and the noise signal components are identified using a spectrum analysis, to achieve further removal of noise information. The results of both simulated and on-site experiments show that the SCBSS signal de-noising method has a powerful signal de-noising ability.

Index Terms—Dynamic deflection, ensemble empirical mode decomposition (EEMD), extreme-point symmetric mode decomposition (ESMD), ground-based synthetic aperture radar (GBSAR), signal de-noising, single-channel blind source separation (SCBSS).

Manuscript received November 13, 2020; revised January 5, 2021 and January 30, 2021; accepted February 20, 2021. Date of publication February 23, 2021; date of current version March 15, 2021. This work was supported in part by the National Natural Science Foundation of China under Grant 41871367, in part by the Ministry of Science and Technology of the People's Republic of China under Grant 2018YFE0206100, in part by the Scientific Research Project of Beijing Educational Committee under Grant KM201910016005, and in part by the Major Projects of Beijing Advanced Innovation Center for Future Urban Design Under Grant UDC2018031321. (Corresponding authors: Xianglei Liu; Yimeng Huang.)

Xianglei Liu is with the Key Laboratory for Urban Geomatics of National Administration of Surveying, Mapping and Geoinformation, Engineering Research Center of Representative Building and Architectural Heritage Database, Ministry of Education, Beijing University of Civil Engineering and Architecture, Beijing 100044, China (e-mail: liuxianglei@bucea.edu.cn).

Hui Wang is with the Beijing University of Civil Engineering and Architecture, Beijing 100044, China (e-mail: 2108160218005@stu.bucea.edu.cn).

Yimeng Huang is with the Beijing University of Civil Engineering and Architecture, Beijing 100044, China (e-mail: 2108570020086@stu.bucea.edu.cn).

Digital Object Identifier 10.1109/JSTARS.2021.3061543

I. INTRODUCTION

IT PLAYS an important role for bridges in transportation networks. However, due to the combination of factors, such as service life, environment, overload, and geological activities, the load-carrying capacity of bridges is gradually decreasing [1]–[3]. In severe cases, it can cause to collapse of bridges suddenly, leading to loss of life and property. Therefore, it is of vital importance for damage detection of bridges. In recent years, with the advantages of noncontact measurements, high-precision, all-weather and all-day measurements, ground-based synthetic aperture radar (GBSAR) technology, as a new measurement technology, has been used extensively for dynamic deflection measurements of bridges [4], [5]. However, complex noise exists in the obtained dynamic deflection of bridges using GBSAR. Among them, the noise is mainly generated by the surrounding environment (such as the interference of vehicles and pedestrians around the equipment to the radar beam), and the equipment itself (equipment internal error), which affects the extraction of useful information in the data analysis, and reduces the accuracy of damage detection [6]. Therefore, it is an essential importance to reduce the influence of noise information in the obtained dynamic deflection of bridges using GBSAR.

At present, the main signal de-noising methods for time-series data include the filtering method [7], [8], the wavelet transform method [9]–[11], and the empirical mode decomposition (EMD) method [12], [13]. The filtering method usually requires prior information about the statistical characteristics of the signal and noise [8]. Therefore, without any prior information, the filtering method is not suitable for signal de-noising of the nonstationary dynamic deflection obtained by GBSAR. The wavelet transform method is easily affected by the choice of wavelet basis, and different noise frequency scales require different wavelet threshold criteria. It needs to set wavelet threshold and choose wavelet basis artificially, which leads to a lack of self-adaptability, and is not suitable for nonlinear signals [11]. In this study, if the monitored bridge was damaged, it should be a nonlinear signal for the obtained dynamic deflection. In addition, it is difficult to determine the appropriate wavelet basis and wavelet threshold criteria. The EMD method can adaptively decompose a nonstationary signal into a series of intrinsic mode functions (IMFs) [12]. However, the decomposed IMFs have the problem of mode mixing, which may result in a loss of accuracy [13]. To solve the problem of mode mixing, the ensemble empirical mode

decomposition (EEMD) method is proposed, which takes the EMD method as the core and inherits the advantages of the EMD method [14]. The EEMD method repeatedly decomposes the original signal with the added white noise into a series of IMFs and further calculates the average value of multiple decomposed IMFs to alleviate mode mixing, which has been widely used in the field of signal de-noising [15]. Moreover, the extreme-point symmetric mode decomposition (ESMD) method, proposed by Wang and Li [16], is a new time-frequency analysis method and a new development of the EMD method. This method can adaptively determine the optimal global mean curve, thereby decomposing any complex original signal into a series of different physical meaning IMFs, which is now widely used for signal de-noising in the fields of information science, ocean and atmospheric science, economics, and seismology [17]. The traditional EMD de-noising method, EEMD de-noising method, and ESMD de-noising method reduce the influence of noise by eliminating a certain number of low-order IMFs with relatively high frequencies [13], [15], [18]. However, there will inevitably be low-frequency noise and some residual high-frequency noise in the remaining IMFs, and it is difficult to remove the influence of possible low-frequency noise using the above three methods directly.

The blind source separation (BSS) algorithm can be used to obtain the estimation of the source signal based on the observed signals with little or no prior knowledge. Recently, it has been widely used in wireless communication, biomedicine, speech signal processing, and signal de-noising [19], [20]. In this study, it is a complicated nonstationary time-series displacement that mixes the useful signal with noise for the obtained dynamic deflection of bridges using GBSAR. Therefore, noise information can be regarded as an independent source signal. The useful information and noise information can be extracted from the original observation data using the BSS method, which can eliminate the influence of noise for the original observation data. According to the relationship between the number of sensors and the number of source signals, the BSS method can be divided into the overdetermined BSS method (the number of sensors is greater than the source signal), the positive determined BSS method (the number of sensors is equal to the source signal), and the underdetermined BSS method (the number of sensors is less than source signal) [21]. However, limited by equipment prices and on-site environment, it is difficult to carry out simultaneous dynamic deflection measurement of bridges using multiple GBSAR instruments. Only a sensor is used to obtain the dynamic deflection of bridges. Therefore, single-channel blind source separation (SCBSS) has become a research hotspot, which is an extreme case of the undetermined BSS method, using a single sensor to receive multiple source signals and perform the separation. It is now widely used in the biomedicine and acoustic monitoring field [22]–[25].

In general, SCBSS can be divided into three separation methods, including the signal parameter differences method [24], [25], the transform domain filtering method [26], [27], and the virtual multichannel method [28]–[31]. The signal parameter differences method uses the difference of component signals on a certain parameter (time-delay, amplitude, frequency, etc.) to

select an algorithm to perform SCBSS [25]. Therefore, without any prior information, the signal parameter differences method is not suitable for signal de-noising of the nonstationary dynamic deflection obtained using GBSAR. The transform domain filtering method maps the mixed signal to a single domain or a joint domain through some reversible transformation, finds the difference of the source signal in this domain, and constructs a filter in this domain to separate each source signal [26]. However, this method also needs the prior information on the statistical characteristics of signal and noise, and the results are easily affected by the different filters [27]. The virtual multichannel method is to convert the single-channel mixed signal into virtual multichannel signals through mathematical transformation, so that it meets the conditions of the classic BSS algorithm and realizes the separation of source signals [28], [29]. Compared with the previous two methods, the virtual multichannel separation method has a wider adaptability, which does not need to target a specific signal, and does not need to rely on the *a priori* characteristics of the signal. This method now mainly includes the space-time method [23]–[28], the over-sampling method [29], the singular spectrum analysis (SSA) method [22], and the time-frequency domain analysis method [30]–[33]. The space-time method is to obtain the multichannel data by delaying the observed single-channel mixed signal. However, the results are easily affected by the choice of delay data, and the separation effect is poor when the mixed signal spectrum is close [28]. The oversampling method is to obtain multichannel data by fractional interval resampling method. The greater the sampling frequency of this method, the better the signal quality. However, the increase in sampling frequency leads to slower algorithm convergence and this method is suitable for stationary signals [29]. The SSA method converts 1-D time-series data into multidimensional series with principal component analysis to obtain different components, and selects several components to reconstruct multiple required data sets, which is suitable for nonlinear data analysis in this study. However, the SAA method needs to manually set the window function size [22].

The time-frequency domain analysis method decomposes single-channel data to obtain multichannel data according to the signal frequency characteristics, such as the wavelet decomposition method [30] and the EMD method [31]. The wavelet decomposition method uses the wavelet basis function to decompose the original single-channel signal into subcomponents of each frequency, and then reconstruct the subcomponent signals separately to obtain multipath signals [30]. The EMD method can adaptively decompose the signal into a series of IMFs, and select the appropriate IMFs and original data to form a multichannel signal [12], [31]. The common point of the above two methods is that the original observation signal is mapped to a multidimensional space through a certain method to obtain multiple components, and the components of interest are selected from the original observation signal to form multiple signals for BSS [30]–[33]. However, the components selected by these methods cannot contain all the features of useful information, which will cause the loss of some data details.

The EEMD and ESMD methods can adaptively decompose the signal into a series of IMFs from high frequency to low

frequency, which can also reduce the influence of mode-mixing problem. Furthermore, due to different interpolation methods (EEMD uses external envelope interpolation, while ESMD uses internal pole symmetric interpolation), it should be different for the decomposed IMFs by the EEMD and ESMD methods, respectively, and the high-frequency noise-dominated IMFs will be also different. Therefore, aiming to reduce the influence of noise information in the dynamic deflection of bridges obtained using GBSAR effectively, an SCBSS signal de-noising method of integrating the EEMD and ESMD methods is proposed for dynamic deflection of bridges using GBSAR in this study. The ESMD and EEMD methods are used to decompose the obtained dynamic deflection signal (the original observation signal) by GBSAR into a series of IMFs and a residual R . Spearman's Rho is used to remove the low-order IMFs to eliminate the influence of high-frequency noise. The remaining IMFs and R decomposed by the ESMD and EEMD methods are reconstructed to obtain two sets of new signals. The two new signals are combined with the original observation signals to form three virtual multichannel signals, which contain the same useful information. The BSS method is used to separate the above three virtual multichannel signals to obtain the separated signal components, and extract useful information from the separated signal components to further remove low-frequency noise and some residual high-frequency noise.

II. METHODS

A. Blind Source Separation

BSS technique can separate multiple source signals acquired in the same time domain by multiple sensors without any prior information—even when the mixed model of different signals is unknown. For instantaneous linear BSS system model, $S(t) = [s_1(t) s_2(t) \dots s_n(t)]^T$ represents n statistically independent unknown source signals. $X(t) = [x_1(t) x_2(t) \dots x_m(t)]^T$ denotes m observation signals, and $N(t) = [n_1(t) n_2(t) \dots n_m(t)]^T$ are channel interference noise [19], [34], [35]. Then, an instantaneous linear BSS system model can be described as follows:

$$X(t) = A \times S(t) + N(t) \quad (1)$$

where A denotes an $m \times n$ mixing matrix. In actual processing, channel interference noise can be regarded as an independent source signal. Therefore, the linear mixed model can also be described as follows:

$$X(t) = A \times S(t). \quad (2)$$

The essence of BSS is to find a separation matrix B , so that $Y(t) = BX(t)$ is an optimal estimate of the source signal, which is obtained from the original observation signal $X(t)$ through the separation matrix B . It can be seen from (2) that only when matrix A is a nonsingular matrix, that is, $m \geq n$, there is a matrix B to realize the separation of the original observation signal $X(t)$ to obtain the estimate of the source signal $Y(t)$ [32]. Therefore, in order to achieve blind separation of different source signals, the number of input observation signals must be greater than or equal to the number of separated source signals.



Fig. 1. Flowchart of the proposed de-noising method for the obtained dynamic deflection of bridges using ground-based synthetic aperture radar (GBSAR).

B. Single-Channel Blind Source Separation

In this study, limited by the price of the equipment and on-site environment, only a nonlinear and nonstationary signal for the dynamic deflection of bridges can be obtained by GBSAR. The EEMD and ESMD methods can adaptively decompose the nonlinear and nonstationary signal with the time-frequency characteristics of the signal [33]. Therefore, for the dynamic deflection data obtained by GBSAR, this study proposes an SCBSS signal de-noising method of integrating EEMD and ESMD methods. Fig. 1 shows the entire workflow of the proposed signal de-noising method for the obtained dynamic deflection of bridges using GBSAR, which includes the following three technologies: 1) The original observation signal is decomposed into a series of IMFs through the EEMD and ESMD methods, respectively, and the Spearman's Rho is calculated to remove the low-order IMF dominated by high-frequency noise; 2) the remaining IMFs are reconstructed to obtain two new sets of signals, which form the three virtual multichannel data with the original observation signals; and 3) the BSS method is used to separate new virtual multichannel signals to eliminate low-frequency noise and some residual high-frequency noise.

1) Reduction of Low-Order IMFs Dominated by High-Frequency Noise: The EEMD method uses the statistical characteristics of Gaussian white noise with uniform frequency distribution and external envelope interpolation, which can obtain a series of IMFs by repeatedly decomposing the original signal with added white noise, and further calculates the average value of multiple decomposed IMFs to reduce mode mixing [14]. The ESMD method is the latest adaptive signal time-frequency processing method developed based on the EMD method. This method innovatively proposes to change the external envelope interpolation to the internal pole symmetric interpolation. It uses "least squares" to optimize the last remaining modes to make them the "adaptive global mean (AGM) curve" of the entire

data, which can not only decompose the original signal into a series of physically meaningful IMFs, but also effectively reduce the mode-mixing effect [16], [18]. Therefore, in this study, the EEMD and ESMD method are used to decompose the dynamic time-series displacement data of bridges collected by GBSAR. For a given dynamic deflection data $X(t)$, the detailed steps of the EEMD signal decomposition method are shown as follows.

Step 1: Add a Gaussian white noise signal $w(t)$ with a mean value of zero, a constant standard deviation, and the same length to the signal $X(t)$ multiple times to obtain a signal containing Gaussian white noise $X'(t) = X(t) + w(t)$.

Step 2: The signal containing Gaussian white noise $X'(t)$ is decomposed by the EMD method to obtain a series of IMF and residual R.

Step 3: Steps 1 and 2 are each repeated N times, and a different Gaussian white noise $w(t)$ is added on each time.

$$X'_i(t) = \sum_{k=1}^n IMF_{i,k}(t) + R_i(t), (i = 1, 2, \dots, N). \quad (3)$$

Step 4: Take the average of the corresponding IMFs components obtained by the N time's decomposition to eliminate the Gaussian white noise component of each IMFs component, and the IMFs component after EEMD decomposition is obtained as (5).

$$IMF_i(t) = \frac{1}{N} \sum_{k=1}^N IMF_{i,k}(t) + R_k(t), (k = 1, 2, \dots, n) \quad (4)$$

$$X(t) = \sum_{k=1}^n IMF_k(t) + R(t). \quad (5)$$

For a given dynamic deflection data $X(t)$, the detailed steps of the ESMD signal decomposition method are shown as follows.

Step 1: Find all the local maxima and minima of the signal $X(t)$, and mark the midpoint of two adjacent extreme points as $F_i (i = 1, 2, \dots, n - 1)$. Add the midpoints F_0 and F_n of the left and right boundaries by a certain approach.

Step 2: Use cubic spline interpolation to construct p interpolation curves $L_1, L_2, \dots, L_p (p \geq 1)$ for these $n + 1$ points, and further calculate the average curve $\bar{L} = (L_1 + L_2 + \dots + L_p) / p$.

Step 3: Repeat the above two steps and calculate $X(t) - \bar{L}$ to obtain IMF_1 until $|\bar{L}| \leq \varepsilon$ (ε is a permitted error). Generally, we choose the permitted error $\varepsilon = 0.001\sigma_0$, where σ_0 is the variance of the original data $X(t)$ or the sifting times reached the preset maximum K (K is an adjustable parameter, which can be set according to the data).

Step 4: Repeat the above three steps for the remaining $X(t) - IMF_1$ to get IMF_2, \dots, IMF_n , until the last residual R—with no more than a certain number of extreme points.

Step 5: Change the sifting times K on a finite integer interval $[K_{\min}, K_{\max}]$, and repeat steps 1–4. Then, calculate the variance σ^2 of $X(t) - R$, find the minimum value of σ / σ_0 in the

range of $[K_{\min}, K_{\max}]$, and obtain the optimal sifting time K_0 , where σ_0 was the standard deviation of the signal $X(t)$.

Step 6: Finally, the above five steps are repeated using the optimal sifting times K_0 to perform optimal signal decomposition for the dynamic deflection data $X(t)$ to obtain a series of IMFs with the optimal AGM curve.

In order to determine the boundary position between the noise-dominated IMFs and the signal-dominated IMFs, Spearman's Rho are used to obtain the position of the demarcation point. For each IMF, the noise-dominated IMF has a small correlation with the original signal, while the signal-dominated IMF has a large correlation. Therefore, in this study, the Spearman's Rho has calculated the correlation between each IMF and the original signal by using (6), which is between $[-1, 1]$. The bigger the coefficient value, the more similar it was to the original signal [11], [36].

$$SP(i) = \rho(X(t), IMF_i(t)) = 1 - \frac{6 \sum_{i=1}^N (X(t) - IMF_i(t))^2}{(N^2 - 1)N} \quad (6)$$

where IMF_i is the i th IMF ($i = 1, 2, \dots, n$), and N is the number of elements of the original signal. When i th is the first minimum value of Spearman's Rho, that is, the correlation between the IMF and the original signal gradually decreases to the gradually increasing demarcation point, which is the demarcation point between the noise-dominated IMFs and the signal-dominated IMFs.

2) *Construction of Virtual Multichannel Data:* To solve the problem of SCBSS, it is necessary to convert single-channel data into multichannel data. Therefore, this study expands the data channel by constructing a virtual multichannel method to meet the requirements of multidata input for BSS.

The original observation data $X(t)$ is decomposed into a series of IMFs and a residual R through the EEMD and ESMD methods. After removing the high-frequency noise, the remaining IMFs are reconstructed by using (7) and (8) to obtain two sets of new signals, which are combined with the original observation signals $X(t)$, to form virtual multichannel signals, $X_{\text{New}}(t) = [X(t), X_{\text{EEMD}}(t), X_{\text{ESMD}}(t)]^T$.

$$X_{\text{EEMD}}(t) = \sum_{i=i_{th}^{\text{eemd}}+1}^{n_e} imf_i(t) + R \quad (7)$$

$$X_{\text{ESMD}}(t) = \sum_{i=i_{th}^{\text{esmd}}+1}^{n_s} imf_i(t) + R \quad (8)$$

where imf_i is the i th IMF ($i = 1, 2, \dots, n$), n_e and n_s are the number of remaining IMFs after reduction of low-order IMFs dominated by high-frequency noise for the original observation signals by using the EEMD and ESMD methods, respectively, and i_{th}^{eemd} and i_{th}^{esmd} are the demarcation point between signal-dominated IMFs and high-frequency noise-dominated IMFs decomposed by the EEMD and ESMD methods, respectively.

3) *Reduction of Low-Frequency Noise and Some Residual High-Frequency Noise:* Although the removal of low-order

IMFs dominated by high-frequency noise reduces the influence of noise, there will inevitably be low-frequency noise and some residual high-frequency noise in the remaining IMFs. The EEMD and ESMD methods are two new developments of the EMD method, both of which can adaptively decompose signals and solve the problem of modal mixing. However, due to different interpolation methods (EEMD uses external envelope interpolation, while ESMD uses internal pole symmetric interpolation), the IMFs obtained by decomposing the same signal will be different. The second-order blind identification (SOBI) algorithm uses joint approximation diagonalization to process the covariance matrix, which can solve the best estimation of the source signal and the mixing matrix, and further obtain the separated signal components from different source signals. It is a relatively robust blind source separation method [19], [37]. Therefore, in this study, after removing high-frequency noise from the IMFs decomposed by the EEMD and ESMD methods, the remaining IMFs are reconstructed to obtain two sets of new signals, which are combined with the original signals to form virtual multichannel data. The SOBI algorithm is used to separate virtual multichannel data, and extract useful information, which can remove low-frequency noise and some residual high-frequency noise. The detailed steps are as follows [19], [35].

- 1) By estimating the sample covariance $R(0)$, in three sets of virtual multichannel signals $X_{\text{New}}(t)$, the maximum eigenvalue of $R(0)$ is denoted as $\lambda_1, \lambda_2, \lambda_3$, and the corresponding eigenvector is denoted as h_1, h_2, h_3 .
- 2) Under the assumption that there is white noise, the estimated value of noise variance σ^2 is the smallest eigenvalue of $R(0)$. Denote $Z(t) = [z_1(t)z_2(t)z_3(t)]^T$ as the whitening signal, where $z_i(t) = (\lambda_i - \sigma^2)^{-\frac{1}{2}} h_i * x(t), i = 1, 2, 3$. The whitening matrix W is shown as follows:

$$W = [(\lambda_1 - \sigma^2)^{-\frac{1}{2}} h_1, \dots, (\lambda_3 - \sigma^2)^{-\frac{1}{2}} h_3]^T. \quad (9)$$

- 3) Whitening the virtual multichannel signal $X_{\text{New}}(t)$ through the whitening matrix W to remove the second-order correlation between signal components

$$Z(t) = W \times X_{\text{New}}(t) = W \times A \times S(t) = V \times S(t). \quad (10)$$

- 4) Calculate the sample covariance matrix $R(\tau) = E[Z(t)Z^T(t + \tau)] = AR_Z(\tau)A^T$ by using the whitened data $Z(t)$, where $\tau \in \{\tau_j | j = 1, 2, \dots, k\}$ is the fixed time delay.
- 5) For all $R(\tau_j)$, the orthogonal matrix V is calculated by the joint approximate diagonalization algorithm.
- 6) Using $Y(t) = BX_{\text{New}}(t) = V^T W X_{\text{New}}(t)$ to obtain the estimated value of the source signal, the mixing matrix A is estimated by $A = W^{-1}V$, where W^{-1} is the pseudo-inverse matrix of the whitening matrix W .
- 7) Use fast Fourier transform to perform time-frequency conversion on the separated signal components, and combine frequency analysis to determine noise components. The reverse reconstruction of the separated signal components

is realized by the estimated value of the mixing matrix A

$$Y_N(t) = A \times Y_Z(t) \quad (11)$$

where $Y_N(t)$ is the reconstructed signal component as the de-noised signal; and $Y_Z(t)$ is a source signal matrix acquired through zeroing the noise signal components in the estimated value of the source signal $Y(t)$.

C. Accuracy Assessment

In order to evaluate the noise reduction effect of the method proposed in this study, four objective evaluation indexes were used, including the noise rejection ratio (NRR) [38], ratio of the variance root (RVR) [18], the noise mode (NM) [39], [40], and the signal energy ratio (SER) [39], [40].

NRR can reflect the ability to resist interference and improve signal-to-noise ratio (SNR). NRR is defined as

$$\text{NRR} = 10(\lg \delta_1^2 - \lg \delta_2^2) \quad (12)$$

where δ_1 and δ_2 are the quasi-deviations of the signals before and after signal de-noising, respectively.

RVR reflects the ratio of the variance root of the denoised signal to the variance root of the original signal difference. RVR is defined as

$$\text{RVR} = \frac{\sum_{i=1}^{N-1} [y(i+1) - y(i)]^2}{\sum_{i=1}^{N-1} [s(i+1) - s(i)]^2}. \quad (13)$$

SER and NM are two indicators considered from the energy point of view. SER reflects the energy similarity between the original signal and the denoised signal, and NM reflects the overall noise level. The SER and NM are defined as

$$\text{SER} = \sqrt{\sum_{i=1}^N y^2(i)} / \sqrt{\sum_{i=1}^N s^2(i)} \quad (14)$$

$$\text{NM} = \sqrt{\sum_{i=1}^N (y(i) - s(i))^2} \quad (15)$$

where $s(i)$ represents the original observation signal; $y(i)$ represents the signal after noise reduction; and N represents the number of sampling points.

Generally, the larger the NRR and NM values are, the smaller the RVR value is, and the closer the SER value is to one, the better the noise reduction effect is.

III. EXPERIMENTS AND ANALYSIS

A. Simulation Example

It is a nonstationary signal composed of useful information and noise for the dynamic deflection of bridges obtained by GBSAR. Therefore, to validate the feasibility of the proposed signal de-noising method, a simulated original signal $x(t)$ is constructed, which includes useful signals (consisting of a nonstationary signal $s_1(t)$ and a stationary signal $s_2(t)$), $s(t) = s_1(t) + s_2(t)$, and a white Gaussian noise signal $n(t)$ with a SNR of 20 dB to make the simulated signal closer to the dynamic deflection obtained using GBSAR. The waveforms of

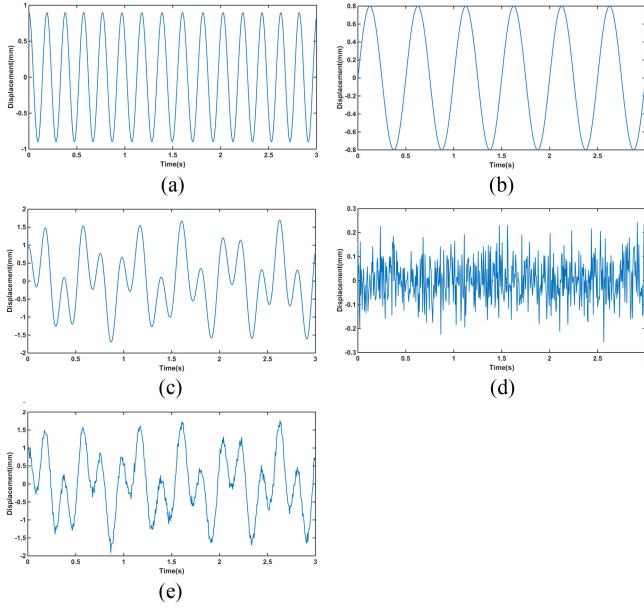


Fig. 2. Waveforms of the simulated signal. (a) Curve of the signal $s_1(t)$. (b) Curve of the signal $s_2(t)$. (c) Curve of the simulated useful signal $s(t)$. (d) Curve of the white Gaussian noise signal $n(t)$. (e) Curve of the simulated original signal $x(t)$.

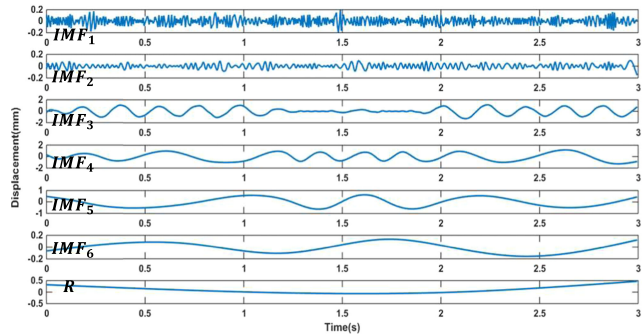


Fig. 3. The simulated original signal $x(t)$ is decomposed into a series of IMFs components and an AGM curve R by the ESMD method.

the simulated signals are shown in Fig. 2.

$$\begin{cases} s_1(t) = 0.9\cos(10\pi t + \sin(2t)) \\ s_2(t) = 0.8\sin(4\pi t) \end{cases} \quad (16)$$

$$x(t) = s(t) + n(t) \quad (17)$$

where the sampling point is 1000, and the sampling frequency is 200 HZ.

The simulated original signal $x(t)$ is decomposed into six IMFs and an AGM curve R by the ESMD method. The results are shown in Fig. 3. The Spearman's Rho of each IMFs component obtained by the ESMD decomposition method and the simulated original signal $x(t)$ is calculated using (6), and the results are shown in Table I. The value of Spearman's Rho gradually decreases from the first decomposed IMF_1 , reaches the first minimum value at IMF_2 , which is 0.0331, and then begins

TABLE I
SPEARMAN'S RHO BETWEEN THE IMF OBTAINED BY ESMD DECOMPOSITION AND THE SIMULATED ORIGINAL SIGNAL

	IMF_1	IMF_2	IMF_3	IMF_4
Spearman's Rho	0.0726	0.0331	0.6452	0.6057
	IMF_5	IMF_6	R	
Spearman's Rho	0.2460	-0.0641	-0.0134	

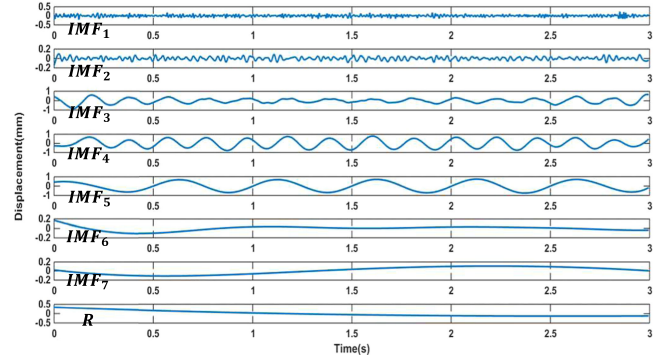


Fig. 4. Simulated original signal $x(t)$ decomposed into a series of IMFs components and residual R by the EEMD method.

TABLE II
SPEARMAN'S RHO BETWEEN THE IMF OBTAINED BY EEMD DECOMPOSITION AND THE SIMULATED ORIGINAL SIGNAL

	IMF_1	IMF_2	IMF_3	IMF_4
Spearman's Rho	0.0650	0.0607	0.6875	0.8110
	IMF_5	IMF_6	IMF_7	R
Spearman's Rho	0.6377	0.1286	0.0060	0.0649

to increase. As described in Section II, IMF_2 is the demarcation point between noise-dominated IMFs and signal-dominated IMFs. Therefore, the first two IMFs are considered to be noise-dominated IMFs and removed. The remaining IMF_2 - IMF_6 and R are reconstructed as a new signal $X_{ESMD}(t)$, to remove the influence of high-frequency noise.

Similarly, by the EEMD method, the simulated original signal $x(t)$ is decomposed into 7 IMFs and a residual R, as shown in Fig. 4. The results of each IMF Spearman's Rho are shown in Table II, IMF_2 is the first minimum value, which is 0.0607. Therefore, the first two IMFs are considered to be noise-dominated IMFs and removed. The remaining IMF_2 - IMF_7 and R are reconstructed as a new signal $X_{EEMD}(t)$, to remove the influence of high-frequency noise.

For the reconstructed signal $X_{EEMD}(t)$ and $X_{ESMD}(t)$, although both remove the influence of high-frequency noise on the signal, there may still be low-frequency noise and some residual high-frequency noise. However, the two reconstructed signals contain all the characteristics of the useful signal. Therefore, the two reconstructed signals $X_{EEMD}(t)$, $X_{ESMD}(t)$ and the simulated original signal $x(t)$ form virtual multichannel data $X_{New}(t)$, as shown in Fig. 5, and the SOBI method is used to extract useful signal components from it to further remove

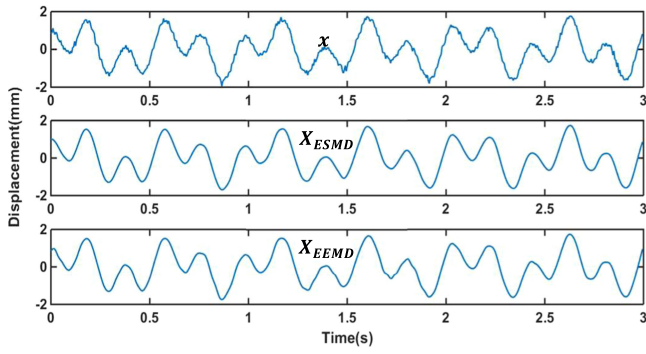


Fig. 5. Virtual multichannel data $X_{New}(t)$, which include the simulated original signal $x(t)$, $X_{ESMD}(t)$, and $X_{EEMD}(t)$.

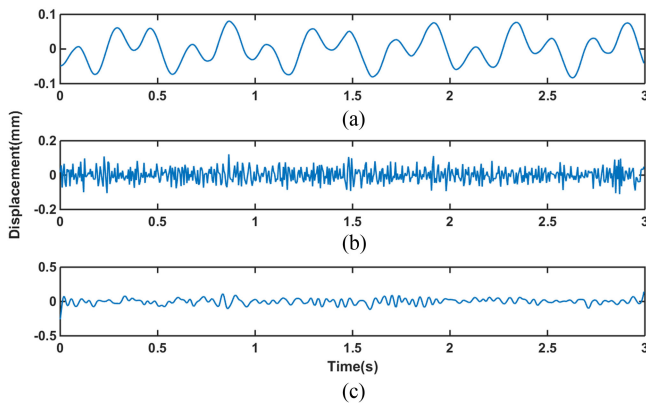


Fig. 6. Separated signals using the SOBI method. (a) Separated signal S1. (b) Separated signal S2. (c) Separated signal S3.

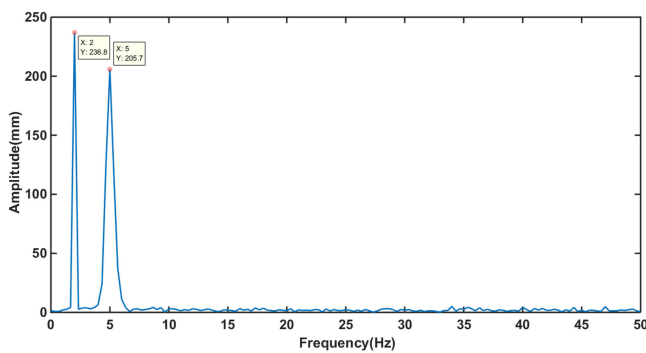


Fig. 7. Spectra of the simulated original signal $x(t)$.

the influence of low-frequency noise and some residual high-frequency noise on the signal. Fig. 6 shows the result of SOBI separation of virtual multichannel data. The inspection of curves of the separated signal components shown in this figure clearly highlights that: (1) as shown in Fig. 6(a), the separated signal S1, with an inverted displacement is consistent with the simulated original signal $x(t)$, which can be regarded as the useful signal; (2) as shown in Fig. 6(b) and (c), the two curves of the separated S2 and S3 signals are disorderly in the whole time domain, which can be regarded as noise signals. In addition, as shown in Fig. 7,

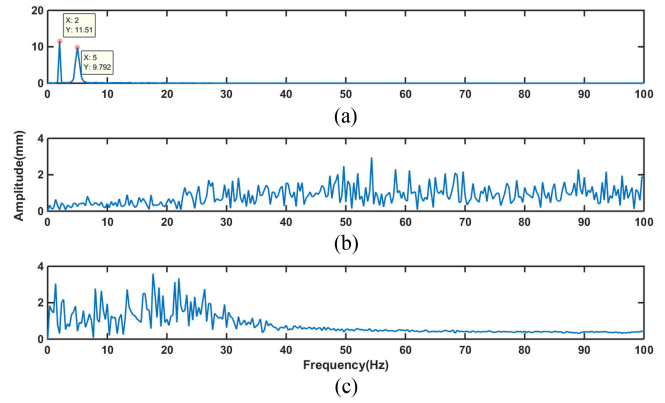


Fig. 8. Spectra of the separated signals using the SOBI method. (a) Spectra of the separated signal S1, (b) Spectra of the separated signal S2, and (c) Spectra of the separated signal S3.

the main frequency of the simulated original signal $x(t)$ is 2 Hz and 5 Hz. The spectra of the separated signal S1 obtained using the SOBI method has the same main frequency as the simulated original signal $x(t)$, as shown in Fig. 8(a), which indicates that the separated signal S1 is a useful signal. However, for the spectra of the separated signals S2 and S3 discovered using the SOBI method, the frequency is disordered and irregular, and the frequency peak of separated signal S2 is concentrated between 30-100Hz, and the frequency peak of separated signal S3 appears between 0-30Hz, as shown in Fig. 8(b) and (c). This indicates that the separated signals S2 and S3 are noise signals, and separated signal S2 is the high-frequency noise, and separated signal S3 is the low-frequency noise.

Then, the separated noise signal S2 and S3 are zeroed, and the separated signals after zeroed is reversely reconstructed by the mixed matrix to obtain the denoised signal, as shown in Fig. 9(a). The red curve is the simulated original signal $x(t)$, and the blue curve is the denoised signal. Compared with the simulated original signal $x(t)$, the denoised signal is more stable and smoother. In order to show the effect of noise reduction more intuitively, Fig. 9(b) shows the comparison between the denoised signal and the useful signal $s(t)$. The denoised signal removes the influence of noise information while retaining the characteristics of the useful signal $s(t)$. However, in some peaks and bottom of the two curves, the denoised signal is slightly different from the useful signal $s(t)$, which may be caused by the calculation error of the reconstruction matrix of the BSS algorithm. The results show that the noise information was effectively eliminated using the proposed signal de-noising method.

Two objective indicators, SNR and root-mean-square error (RMSE), are used to evaluate the noise reduction effect of the method proposed in this article [11]. SNR is the ratio of signal power to noise power, which can reflect the de-noising ability of the algorithm, as shown in (18). RMSE is the deviation value between the observed value and the true value, which can reflect the difference between the original signal and the denoised signal, as shown in (19). Generally, the larger the SNR value is, and the smaller the RMSE value is, the better the noise reduction

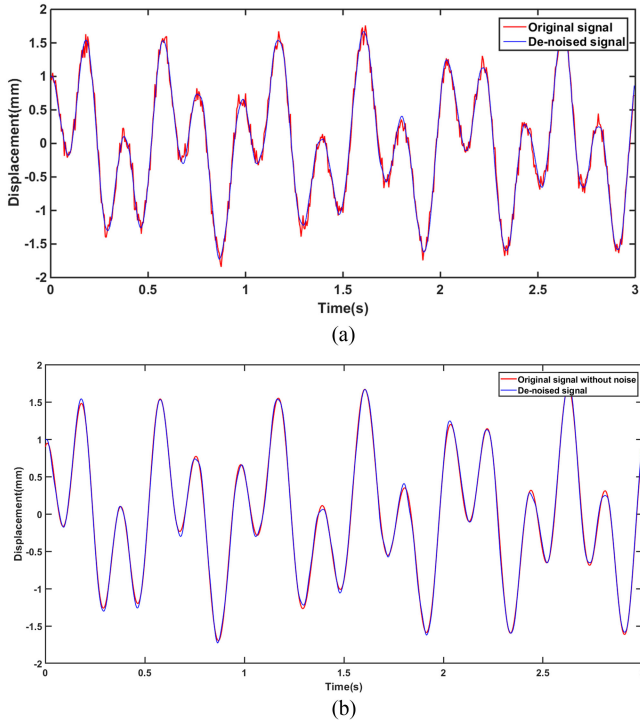


Fig. 9. Comparison between the simulated original signal $x(t)$, the simulated useful signal $s(t)$, and the denoised signal. (a) Comparison between the simulated original signal $x(t)$ and the denoised signal, (b) Comparison between the denoised signal and the simulated useful signal $s(t)$.

TABLE III
COMPARISON OF THE TWO EVALUATION INDEXES AMONG THE THREE
DENOISED METHODS

Index	EEMD	ESMD	Proposed method
SNR (dB)	26.3032	26.4976	27.0422
RMSE (mm)	0.0412	0.0403	0.0378

effect is.

$$\text{SNR} = 10 \log \left(\frac{\sum_{i=1}^N (s(i))^2}{\sum_{i=1}^N (y(i) - s(i))^2} \right) \quad (18)$$

$$\text{RMSE} = \sqrt{\frac{1}{N} \sum_{i=1}^N (y(i) - s(i))^2} \quad (19)$$

where $s(i)$ represents the original signal, $y(i)$ represents the denoised signal, and N represents the number of sampling points.

Table III shows the comparison results of three methods, including the method proposed in this article, the EEMD signal de-noising method, and the ESMD signal de-noising method. The inspection from this table highlights that (1) the SNR was 27.0422 dB for the proposed signal de-noising method, which is much better than that of the EEMD and ESMD methods, and (2) the RMSE was 0.0378 mm for the proposed signal de-noising method, which was smaller and closer to zero than that of the EEMD and ESMD methods. In summary, the SNR and RMSE of the proposed signal de-noising method in this article are increased by 2.8% and 9%, respectively, compared with the EMD

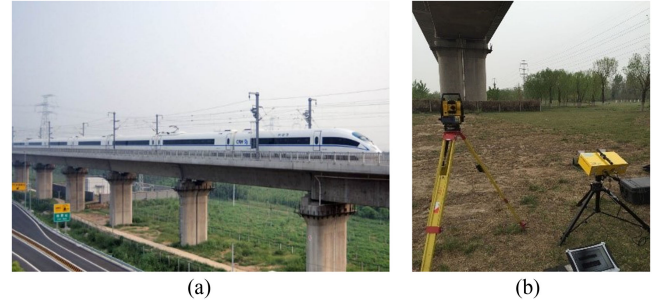


Fig. 10. The Beijing-Tianjin Intercity Railway Bridge and the IBIS-S instrument layout. (a) The Beijing-Tianjin Intercity Railway Bridge and (b) the dynamic deflection measurement of the Beijing-Tianjin Intercity Railway Bridge using IBIS-S.

method, and by 2% and 6.6%, respectively, compared with the EEMD method. Therefore, according to these two indexes, the proposed signal de-noising method had a more powerful ability than the EEMD and ESMD methods for dynamic deflection measurements using GBSAR.

B. On-Site Experiment and Analysis

1) *Experimental Site Description*: Beijing-Tianjin Intercity Railway is an intercity railway connecting Beijing and Tianjin. It is the first high-speed railway with a high standard and a design speed of 350 km/h in China. To validate the accuracy of the proposed signal de-noising method for the dynamic deflection obtained using GBSAR, the *in situ* beam of the Beijing-Tianjin Intercity Railway Bridge was selected as the experimental bridge, with a standard span of 30 m, as shown in Fig. 10(a). The GB-SAR instrument was located under the Beijing-Tianjin Intercity Railway Bridge as shown in Fig. 10(b). This research uses an Imaging by Interferometry Survey (IBIS-S) instrument (including a radar unit, a power supply unit, a control personal computer and a tripod) to obtain the dynamic deflection of the monitored bridge. In typical measurement conditions, the sampling rate can reach 200 Hz, the maximum detection distance can reach 1 km, the distance resolution can reach 0.50 m, and the displacement measurement accuracy can reach 0.01 mm [18]. As shown in Fig. 10, the IBIS-S instrument was located under the Beijing-Tianjin Intercity Railway Bridge, and the angle of the radar unit was set to 32° , so that the two antennas on the radar unit can be aligned with the quarter-span of the bridge. The sampling frequency is 195 Hz, and the data acquisition time is 30 s.

Fig. 11 shows the obtained dynamic deflection X1 of a mid-span point on the Beijing-Tianjin Intercity Railway Bridge. Due to the influences of the surrounding environment and the equipment itself, there was an inevitable increase in the noise information of the obtained dynamic deflection of bridges. Therefore, in order to improve the accuracy of the obtained dynamic deflection of the mid-span point of the Beijing-Tianjin Intercity Railway Bridge, it is necessary to reduce the noise of the dynamic deflection data X1.

2) *De-Noising Results Analysis and Discussion*: The ESMD method is used to decompose the dynamic deflection data X1

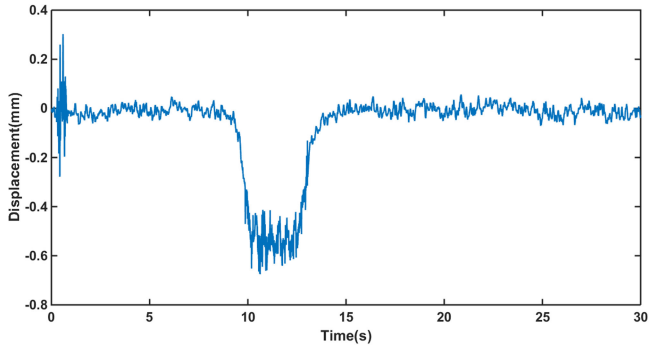


Fig. 11. Dynamic deflection data X1 of a mid-span point on the Beijing-Tianjin Intercity Railway Bridge.

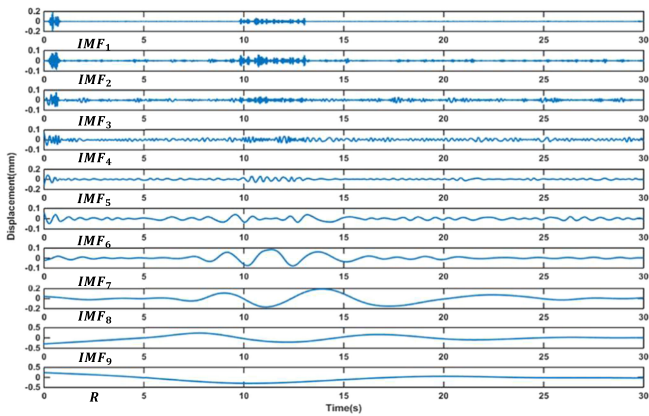


Fig. 12. Dynamic deflection data X1 is decomposed into a series of IMFs components and an AGM curve R by the ESMD method.

 TABLE IV
 SPEARMAN'S RHO BETWEEN THE IMF OBTAINED BY ESMD DECOMPOSITION AND THE DYNAMIC DEFLECTION DATA X1

	IMF_1	IMF_2	IMF_3	IMF_4	IMF_5
Spearman's Rho	0.0898	0.1591	0.2447	0.2686	0.2144
	IMF_6	IMF_7	IMF_8	IMF_9	R
Spearman's Rho	0.2201	-0.0027	0.0728	0.2971	0.4164

into nine IMFs and an AGM curve R, as shown in Fig. 12. The Spearman's Rho of each IMFs component decomposed by the ESMD method and the dynamic deflection data X1 is calculated using (6), and the results are shown in Table IV. As described in Section II, IMF_1 is the demarcation point between noise-dominated IMFs and signal-dominated IMFs. Therefore, the IMF_1 is considered to be the noise-dominated IMF and removed, and the remaining IMF_2 - IMF_9 and R is reconstructed as a new signal, $X1_{ESMD}(t)$, to remove the influence of high-frequency noise on the signal.

The EEMD method is used to decompose the dynamic deflection data X1 into seven IMFs and a residual R, as shown in Fig. 13. The results of each IMF Spearman's Rho are shown in Table V; IMF_1 is the demarcation point between noise-dominated IMFs and signal-dominated IMFs. Therefore, IMF_1 is considered to be the noise-dominated IMF and removed, and

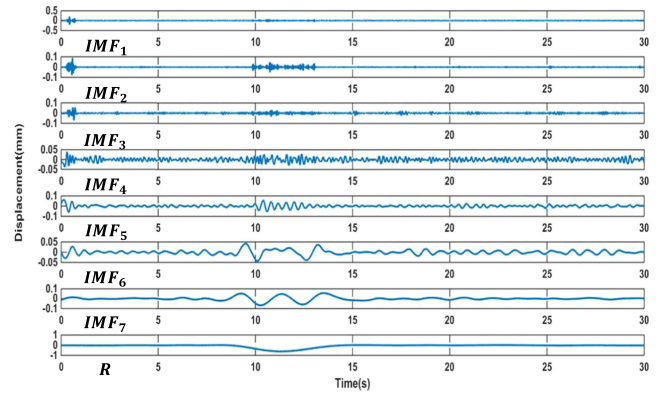
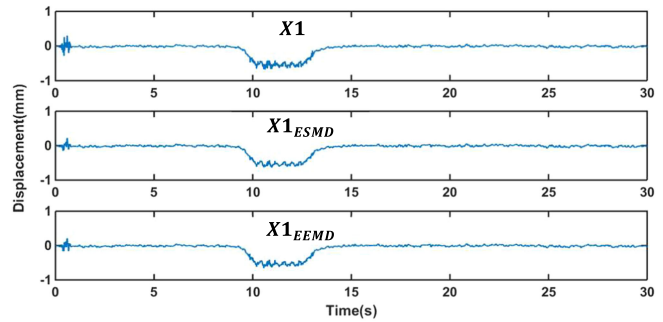


Fig. 13. Dynamic deflection data X1 is decomposed into a series of IMFs components and a residual R by the EEMD method.

 TABLE V
 SPEARMAN'S RHO BETWEEN THE IMF OBTAINED BY EEMD DECOMPOSITION AND THE DYNAMIC DEFLECTION DATA X1

	IMF_1	IMF_2	IMF_3	IMF_4
Spearman's Rho	0.0763	0.1496	0.2813	0.3546
	IMF_5	IMF_6	IMF_7	R
Spearman's Rho	0.3500	0.1755	0.1157	0.6725


 Fig. 14. Virtual multichannel data $X1_{New}(t)$, which include the dynamic deflection data X1, $X1_{ESMD}(t)$, and $X1_{EEMD}(t)$.

the remaining IMF_2 - IMF_7 and R is reconstructed as a new signal, $X1_{EEMD}(t)$, to remove the influence of high-frequency noise on the signal.

Virtual multichannel data $X1_{New}(t)$ is formed using dynamic deflection data X1 and the two reconstructed signals $X1_{EEMD}(t)$, $X1_{ESMD}(t)$, as shown in Fig. 14. The SOBI method is used to extract useful signal components to further remove the influence of low-frequency noise and some residual high-frequency noise. Fig. 15 shows the result of SOBIs separation of virtual multichannel data. The inspection of curves of the separated signal components shown in this figure clearly highlights that 1) as shown in Fig. 15(a), the separated signal, S1, with an inverted displacement is consistent with the dynamic deflection data X1, which can be regarded as the useful signal, and 2) as shown in Fig. 15(b) and (c), there are some sudden changes in the two curves 1s and 10-13s of the separated S2 and S3 signals, which can be considered as noise signals. These may

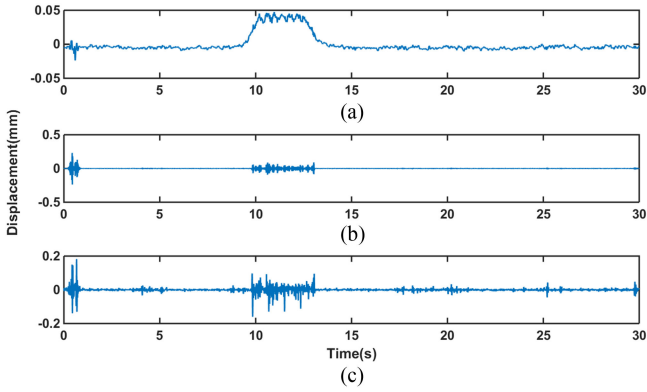


Fig. 15. Separated signals of virtual multichannel data $X1_{New}(t)$ using the SOBI method. (a) Separated signal S1. (b) Separated signal S2. (c) Separated signal S3.

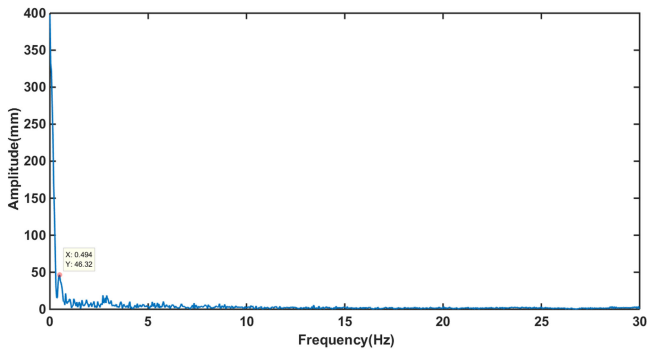


Fig. 16. Spectra of the dynamic deflection X1.

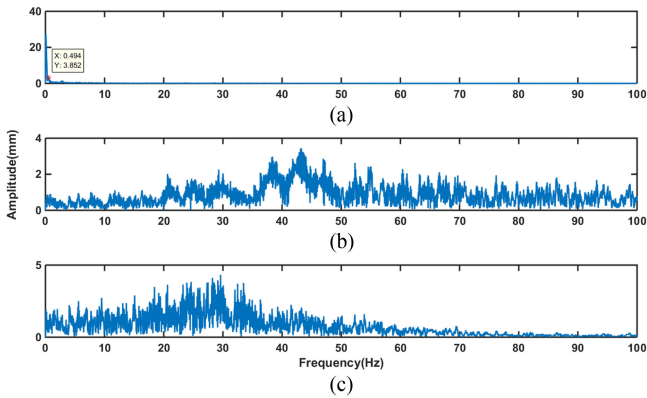


Fig. 17. Spectra of the separated signals using the SOBI method. (a) Spectra of the separated signal S1. (b) Spectra of the separated signal S2. (c) Spectra of the separated signal S3.

be caused by pedestrians near the IBIS-S instrument and sudden overload. In addition, as shown in Fig. 16, the main frequency of the dynamic deflection data X1 is 0.494 Hz. The spectra of the separated signal S1 obtained using the SOBI method is the same as that of the dynamic deflection data X1, as shown in Fig. 17(a), which indicates that the separated signal S1 is a useful signal. However, for the spectra of the separated signals S2 and S3 discovered using the SOBI method, the frequency is

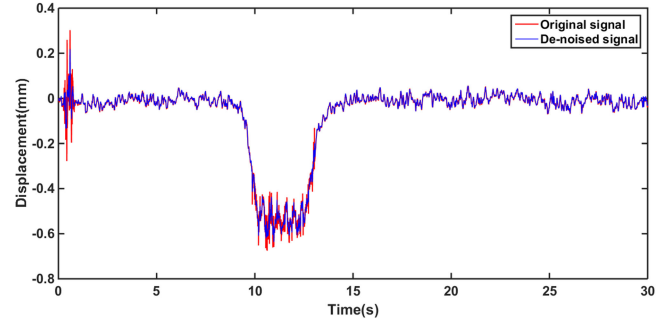


Fig. 18. Denoised dynamic deflection data X1 of the mid-span point of the Beijing–Tianjin Intercity Railway Bridge.

TABLE VI
COMPARISON OF THE FOUR EVALUATION INDEXES AMONG THE THREE
DENOISED METHODS

Index	EEMD	ESMD	Proposed Method
NRR (dB)	3.1303	12.2528	19.0565
RVR (mm)	0.1479	0.2162	0.1401
SER	0.9973	0.9961	0.9951
NM (mm)	0.8297	0.8557	0.9335

disordered and irregular, and the frequency peak of separated signal S2 is concentrated between 30 and 100 Hz, and the frequency peak of separated signal S3 appears between 0 and 40 Hz, as shown in Fig. 17(b) and (c). This indicates that the separated signals S2 and S3 are noise signals, and separated signal S2 is the high-frequency noise, and separated signal S3 is the low-frequency noise.

Then, the separated noise signals S2 and S3 are zeroed, and the separated signals after zeroing is reversely reconstructed by the mixed matrix to obtain the denoised signal, as shown in Fig. 18. The red curve is the dynamic deflection data X1, and the blue curve is the denoised signal. Compared with the dynamic deflection data X1, the denoised signal is more stable and smoother. The results show that the noise information was effectively eliminated using the proposed signal de-noising method.

3) *De-Noising Quality Evaluation*: To validate the accuracy of the proposed signal de-noising method for dynamic deflection obtained using GBSAR, two de-noising methods—EEMD [20] and ESMD [22]—were selected to be compared with the proposed signal de-noising method. The comparison results are shown in Table VI. The inspection from this table highlights the following: 1) the NRR, RVR, and NM are 19.0565 dB, 0.1401 mm, and 0.9335 mm using the proposed signal de-noising method, which are much better than that of the EEMD and ESMD methods. Therefore, according to these three indexes, the proposed signal de-noising method has a more powerful ability than the EEMD and ESMD methods for dynamic deflection measurements using GBSAR. 2) The SER is 0.9951, which is smaller than that of the EEMD and ESMD methods. The reason is that the proposed signal de-noising method removes the noise signal in the low-frequency component, which means that more energy is reduced, resulting in a smaller SER value

compared with the other two methods. Moreover, the NRR is 19.0565 dB for the proposed signal de-noising method, which has a great improvement compared with the EEMD method (3.1303 dB). The reason is that the proposed method combines the advantages of the EEMD and ESMD methods, not only removing high-frequency noise information, but also removing low-frequency noise and possible residual high-frequency noise. However, the EEMD denoised method only removes high-frequency noise information based on Spearman's Rho. The results indicate that the proposed signal de-noising method has a powerful de-noising ability, which can not only reduce high-frequency noise, but also reduce low-frequency noise.

IV. CONCLUSION

The EEMD and ESMD methods can reduce the impact of high-frequency noise by removing low-order IMFS, but there may still be low-frequency noise and some residual high-frequency noise in the remaining IMFs components. A single EEMD or ESMD method cannot remove the influence of low-frequency noise on the signal. However, all the features of useful information are contained in the remaining IMFs components. Therefore, in this study, to improve the accuracy of the obtained dynamic deflection of bridges using GBSAR, the proposed signal de-noising method was proposed to reduce the influence of noise. The original observation signal is decomposed by the ESMD and EEMD methods, respectively. The remaining IMFs and R after removing the low-order IMFs dominated by high-frequency noise are reconstructed to obtain two sets of new signals, which are combined with the original observation signal to form a virtual multichannel signal. The three sets of data contain the same useful information. The BSS method is used to separate new virtual multichannel signals to obtain separated signal components and extract useful information from them, thereby further reducing the impact of noise information. More specifically, the results presented in the study clearly highlight the following.

- 1) A simulation experiment was performed to validate the feasibility of the proposed signal de-noising method. The method uses three sets of simulated source signals with different frequency ranges to linearly mix them to obtain a set of nonstationary and nonlinear signals. The SNR is 27.0422 dB and the RMSE value is 0.0378 mm for the method proposed in this study, which is better than the EEMD and ESMD methods. The results show that the proposed signal de-noising method can effectively reduce the influence of noise information for the nonstationary and nonlinear signals.
- 2) By fully considering the characteristics of EEMD, ESMD, and BSS technology, the remaining IMFs reconstructed by EEMD and ESMD after removing high-frequency noise and the original observation data are selected as the three sets of input signals. The three sets of data also contain all the characteristics of useful information. This was done in order to extract useful information components by using the SOBI method to obtain further denoised dynamic deflection data. The results show that the proposed

signal de-noising method not only eliminates the effects of high-frequency noise but can also reduce the influences of low-frequency noise and some residual high-frequency noise.

- 3) Compared with the EEMD and ESMD signal de-noising methods, the proposed signal de-noising method displayed a greater improvement in the indexes of NRR, NM, and RVR for the obtained dynamic deflection of a bridge using GBSAR. The results indicate that the proposed signal de-noising method has a powerful signal de-noising ability, which not only efficiently reduced the effects of noise for the dynamic deflection signals but could also retain the useful information.

ACKNOWLEDGMENT

The authors would like to thank the reviewers for very constructive and detailed comments.

REFERENCES

- [1] J. M. Ko and Y. Q. Ni, "Technology developments in structural health monitoring of large-scale bridges," *Eng. Struct.*, vol. 27, no. 12, pp. 1715–1725, 2005.
- [2] B. Riveiro, H. Gonzalezjorge, M. E. Varela, and D. V. Jauregui, "Validation of terrestrial laser scanning and photogrammetry techniques for the measurement of vertical underclearance and beam geometry in structural inspection of bridges," *Measurement*, vol. 46, no. 1, pp. 784–794, 2013.
- [3] S. A. Dabous and S. Feroz, "Condition monitoring of bridges with non-contact testing technologies," *Autom. Construction*, vol. 116, 2020, Art. no. 103224.
- [4] O. Monserrat, M. Crosetto, and G. Luzi, "A review of ground-based SAR interferometry for deformation measurement," *ISPRS J. Photogramm. Remote Sens.*, vol. 93, pp. 40–48, 2014.
- [5] G. Granello, K. Andisheh, and A. Palermo, "Microwave radar interferometry as a cost-efficient method of monitoring the structural health of bridges in New Zealand," *Struct. Eng. Int.*, vol. 28, no. 4, pp. 518–525, 2018.
- [6] X. Liu, Z. Lu, W. Yang, M. Huang, and X. Tong, "Dynamic monitoring and vibration analysis of ancient bridges by ground-based microwave interferometry and the ESMD method," *Remote Sens.*, vol. 10, no. 5, p. 770, 2018.
- [7] G. Makwana and L. Gupta, "De-noising of electrocardiogram (ECG) with adaptive filter using MATLAB," in *Proc. Int. Conf. Commun. Syst. Netw. Technol.*, 2015, pp. 511–514.
- [8] H. X. Chen, L. Tu, K. Sun, and C. Liu, "An optimized particle filter for signal de-noising processing," *Key Eng. Mater.*, vol. 589, pp. 629–633, 2013.
- [9] O. Ogundipe, J. K. Lee, and G. W. Roberts, "Wavelet de-noising of GNSS based bridge health monitoring data," *J. Appl. Geodes.*, vol. 8, no. 4, pp. 273–282, 2014.
- [10] S. K. Yadav, R. Sinha, and P. K. Bora, "Electrocardiogram signal de-noising using non-local wavelet transform domain filtering," *IET Signal Proc.*, vol. 9, no. 1, pp. 88–96, 2015.
- [11] X. Liu, M. Jiang, Z. Liu, and H. Wang, "A morphology filter-assisted extreme-point symmetric mode decomposition (MF-ESMD) de-noising method for bridge dynamic deflection based on ground-based microwave interferometry," *Shock Vib.*, vol. 2020, no. 11, pp. 1–13, 2020.
- [12] N. E. Huang *et al.*, "The empirical mode decomposition and the Hilbert spectrum for nonlinear and non-stationary time series analysis," in *Proc. R. Soc. A*, vol. 454, no. 1971, pp. 903–995, 1998.
- [13] G. Han, B. Lin, and Z. Xu, "Electrocardiogram signal de-noising based on empirical mode decomposition technique: An overview," *J. Instrum.*, vol. 12, no. 3, 2017, Art. no. 03010.
- [14] Z. Wu and N. E. Huang, "Ensemble empirical mode decomposition: A noise-assisted data analysis method," *Adv. Adapt. Data Anal.*, vol. 1, no. 1, pp. 1–41, 2009.
- [15] S. Gaci, "A new ensemble empirical mode decomposition (EEMD) de-noising method for seismic signals," *Energy Procedia*, vol. 97, pp. 84–91, 2016.

- [16] J. Wang and Z. Li, "Extreme-point symmetric mode decomposition method for data analysis," *Adv. Adapt. Data Anal.*, vol. 5, no. 3, 2013, Art. no. 1350015.
- [17] J. Wang and X. Fang, "ESMD method for frequency distribution of tank surface temperature under wind effect," *Int. J. Geosci.*, vol. 6, no. 5, pp. 481–486, 2015.
- [18] X. Liu, S. Li, and X. Tong, "Two-level W-ESMD de-noising for dynamic deflection measurement of railway bridges by microwave interferometry," *IEEE J. Sel. Top. Appl. Earth Observ. Remote Sens.*, vol. 11, no. 12, pp. 4874–4883, Dec. 2018.
- [19] A. Belouchrani, K. Abedmeraim, J. F. Cardoso, and E. Moulines, "A blind source separation technique using second-order statistics," *IEEE Trans. Signal Process.*, vol. 45, no. 2, pp. 434–444, Feb. 1997.
- [20] V. Roy and S. Shukla, "Designing efficient blind source separation methods for EEG motion artifact removal based on statistical evaluation," *Wirel. Pers. Commun.*, vol. 108, no. 3, pp. 1311–1327, 2019.
- [21] C. Fevotte and S. J. Godsill, "A Bayesian approach for blind separation of sparse sources," *IEEE Trans. Audio Speech*, vol. 14, no. 6, pp. 2174–2188, Nov. 2006.
- [22] H. Ma, Q. Jiang, Z. Liu, G. Liu, and Z. Ma, "A novel blind source separation method for single-channel signal," *Signal Process.*, vol. 90, no. 12, pp. 3232–3241, 2010.
- [23] P. He, T. She, W. Li, and W. Yuan, "Single channel blind source separation on the instantaneous mixed signal of multiple dynamic sources," *Mech. Syst. Sig. Process.*, vol. 113, pp. 22–35, 2017.
- [24] C. Liao, J. Wan, and S. Zhou, "Single-channel blind separation performance bound of two co-frequency modulated signals," *J. Tsinghua Univ.*, vol. 50, no. 10, pp. 1646–1650, 2010.
- [25] S. Tu, H. Zheng, and N. Gu, "Single-channel blind separation of two QPSK signals using per-survivor processing," in *Proc. Asia Pacific Conf. Circuits Syst.*, 2008, pp. 473–476.
- [26] L. Atlas and C. Janssen, "Coherent modulation spectral filtering for single-channel music source separation," in *Proc. Int. Conf. Acoust. Speech, Signal Process.*, 2005, pp. 461–464.
- [27] J. Ming, T. J. Hazen, and J. Glass, "Combining missing-feature theory, speech enhancement, and speaker-dependent/-independent modeling for speech separation," in *Proc. Conf. Int. Speech Commun. Assoc.*, 2010, pp. 67–76.
- [28] M. E. Davies and C. J. James, "Source separation using single channel ICA," *Signal Process.*, vol. 87, no. 8, pp. 1819–1832, 2007.
- [29] G. Lu, M. Xiao, P. Wei, and J. Li, "Single channel blind separation of oversampling communication signals based on ICA," in *Proc. IEEE Int. Conf. Commun. Problem-Solving*, 2014, pp. 364–367.
- [30] H. Hong and M. Liang, "Separation of fault features from a single-channel mechanical signal mixture using wavelet decomposition," *Mech. Syst. Sig. Process.*, vol. 21, no. 5, pp. 2025–2040, 2007.
- [31] W. U. Wenfeng, "Blind source separation of single-channel mechanical signal based on empirical mode decomposition," *J. Mech. Eng.*, vol. 47, no. 4, p. 12, 2011.
- [32] Y. Zhang, S. Qi, and L. Zhou, "Single channel blind source separation for wind turbine aeroacoustics signals based on variational mode decomposition," *IEEE Access*, vol. 6, pp. 73952–73964, 2018.
- [33] K. Wang, Q. Hao, X. Zhang, Z. Tang, Y. Wang, and Y. Shen, "Blind source extraction of acoustic emission signals for rail cracks based on ensemble empirical mode decomposition and constrained independent component analysis," *Measurement*, vol. 157, 2020, Art. no. 107653.
- [34] W. Zhou and D. Chelidze, "Blind source separation-based vibration mode identification," *Mech. Syst. Sig. Process.*, vol. 21, no. 8, pp. 3072–3087, 2007.
- [35] X. Liu, H. Wang, and Yang, "An improved second-order blind identification (SOBI) signal de-noising method for dynamic deflection measurements of bridges using ground-based synthetic aperture radar (GBSAR)," *Appl. Sci.*, vol. 9, 2019, Art. no. 3561.
- [36] J. Li, Y. Tong, L. Guan, S. Wu, and D. Li, "A UV-visible absorption spectrum de-noising method based on EEMD and an improved universal threshold filter," *RSC Adv.*, vol. 8, no. 16, pp. 8558–8568, 2018.
- [37] J. Seppanen, J. Turunen, M. Koivisto, and L. Haarla, "Measurement based analysis of electromechanical modes with second order blind identification," *Elect. Power Syst. Res.*, vol. 121, no. 121, pp. 67–76, 2015.
- [38] C. Jian-Hua, X. Yong-Liang, and L. I. Xiao-Qin, "Nuclear magnetic resonance logging signal de-noising based on empirical mode decomposition threshold filtering in frequency domain," *Prog. Geophys.*, vol. 34, no. 02, pp. 509–516, 2019.
- [39] L. Lv, W. Gong, S. Song, and B. Zhu, "De-noising process based on wavelet transform in feature reflectance detection LiDAR system," *Geomat. Inf. Sci. Wuhan Univ.*, vol. 36, no. 121, pp. 56–59, 2011.
- [40] L. Lv, "Evaluation system of wavelet de-noising effect for multispectral LiDAR," *Hydrogr. Surv. Chart*, vol. 36, no. 121, pp. 72–75, 2016.



Xianglei Liu received the B.S. and M.S. degrees in geographic information systems from the Shandong University of Science and Technology, Qingdao, China, in 2005 and 2008, respectively, and the Ph.D. degree in photogrammetry and remote sensing from Tongji University, Shanghai, China, in 2012.

He is currently a Professor with Beijing University of Civil Engineering and Architecture, Beijing, China. His research interests include deformation monitoring based on GBSAR and high-speed videogrammetric measurement.



Hui Wang received the B.S. degree in remote sensing science and technology from the Beijing University of Civil Engineering and Architecture, Beijing, China, in 2018, where he is currently working toward the graduate degree in photogrammetry and remote sensing.

His research interests include bridge dynamic deflection signal de-noising based on GBSAR.



Yimeng Huang received the B.S. degree in remote sensing science and technology from Beijing University of Civil Engineering and Architecture, Beijing, China, in 2020, where she is currently working toward the graduate degree in resources and environment.

Her research interests include bridge dynamic deflection signal de-noising based on GBSAR.